Fast 3D simulation of transient electromagnetic fields by model reduction in the frequency domain using Krylov subspace projection

Ralph-Uwe Börner[1], Oliver G. Ernst[2], and Klaus Spitzer[1]
Technische Universität Bergakademie Freiberg, Freiberg, Germany
[1]Institute of Geophysics, [2]Institute of Numerical Analysis and Optimization

1 Summary

We present an efficient numerical method for the simulation of transient electromagnetic fields resulting from magnetic and electric dipole sources in three dimensions.
The method we propose is based on the Fourier synthesis of frequency domain solutions at a sufficient number of discrete frequencies obtained using a finite element (FE) approximation of the damped vector wave equation, which results after Fourier transforming Maxwell's equations in time. We assume the solution to be required only at a few points in the computational domain, whose number is small relative to the number of FE degrees of freedom. The mapping which assigns to each frequency the FE approximation at the points of interest is a vector-valued rational function known as the transfer function. Its evaluation is approximated using Krylov subspace projection, a standard model reduction technique. Computationally, this requires the FE discretization at one reference frequency and the generation of a sufficiently large Krylov subspace associated with the reference frequency. Once a basis of this subspace is available, a sufficiently accurate rational approximation of the transfer function can be evaluated at the remaining frequencies at negligible cost. These partial frequency domain solutions are then synthesized to the time evolution at the points of interest using a fast Hankel transform.
To test the algorithm, responses have been calculated for a three-layered earth and compared with results obtained analytically. We observe a maximum deviation of less than 2 percent in the case of transient EM modelling. We emphasize the usability of our approach by an example of a controlled-source marine electromagnetic application.
A first implementation of our new numerical algorithm already gives very good results using much less computational time compared with time stepping methods and comparable times and somewhat

improved accuracy compared with the Spectral Lanczos Decomposition Method (SLDM).

Keywords: Transient electromagnetic modelling, Krylov projection methods

2 Introduction

The transient electromagnetic (TEM) method has become one of the standard applications in geoelectromagnetism and is now widely used, e.g., for exploration of groundwater and mineral resources. The numerical computation of transient electromagnetic fields is of particular interest in applied geophysics. First introduced by Yee (1966), the finite difference time domain (FDTD) technique has been widely used to simulate the transient fields in 2D and 3D engineering applications by time stepping (Taflove, 1995). In geophysics, first attempts to numerically simulate transients were made by Goldman and Stoyer (1983) for axially-symmetric conductivity structures using implicit time-stepping. Wang and Hohmann (1993) have developed an explicit FDTD method in 3D based on Du Fort-Frankel time-stepping.

Generally, explicit time stepping algorithms require small time steps to guarantee numerical stability. For the simulation of late-time responses their computational cost must therefore be regarded as very high. Several attempts have been made to reduce the numerical effort, e.g., by a special treatment of the air-earth interface to circumvent excessively small time steps due to the extremely low conductivity of the air layer (Oristaglio & Hohmann, 1984; Wang & Hohmann, 1993).

For FDTD methods, it thus seems that acceptable computing times can only be achieved by parallelization using computer clusters (Commer & Newman, 2004).

An alternative approach was introduced by Druskin and Knizhnerman (1988) and has since been known as the Spectral Lanczos Decomposition Method (SLDM). This method uses a 3D finite difference (FD) approximation of Maxwell's equations, which are cast into a system of ordinary differential equations. The solution of the latter is formulated as a multiplication of a matrix exponential and a vector of initial values. Numerical evidence indicates that the convergence of the SLDM depends mainly on the conductivity contrasts within the model. To improve convergence, the FD grids have to be refined near jumps of electrical conductivity within the discretized region. However, the FD tensor product grids further increase the number of unknowns even in regions where densely sampled solutions are not of particular interest, e.g. at greater depths.

We note, however, that the time-stepping technique that is inherent to SLDM can be combined with other

spatial discretizations.

Everett and Edwards (1993) have published a finite element (FE) discretization for the solution of a 2.5-D problem with subsequent Laplace transform of the response of electric dipoles located on the sea floor. A FE solution of geo-electromagnetic problems for 2D sources using isoparametric quadratic elements has been introduced by Mitsuhata (2000) with respect to frequency domain modelling of dipole sources over undulating surfaces.

The approach of modelling in the frequency domain with subsequent transformation into the time domain was proposed by Newman et al. (1986), who used a 3D integral equation method to provide the responses for typically 20 to 40 frequencies, which are transformed into the time domain using a digital filtering technique (Anderson, 1979). However, the time domain results displayed deviations from reference solutions at late times due to the limited accuracy of the 3D responses.

Sugeng et al. (1993) have computed the step response solutions for 31 frequencies over a range between 1 and 1000 kHz using isoparametric finite elements. The authors report small deviations in the late time response.

Jin et al. (1999) have developed a frequency-domain and time-domain FE solution using SLDM for a small bandwidth of frequencies and very short times, respectively.

This paper introduces a method based on a FE discretization in the frequency domain. We avoid the heavy computational expense associated with solving a full 3D problem for each of many frequencies by a model reduction approach. The point of departure is that the transients, which are synthesized from the frequency domain solutions, are required only at a small number of receiver locations. The synthesis of the transients at these locations therefore requires only frequency domain solutions at these points. After discretization in space, the frequency domain solution values at the receiver points are rational functions of frequency. Using the model reduction technique of Krylov subspace projection (cf. (Antoulas, 2005)) it is possible to approximate this function, known as the *transfer function* in linear systems theory, by rational functions of lower order. Computationally, the discretized frequency-domain problem for a suitably chosen reference frequency is projected onto a Krylov subspace of low dimension, yielding the desired approximation of the transfer function in terms of quantities generated in the Arnoldi process, which is used to construct an orthonormal basis of the Krylov subspace. This approximation, the evaluation of which incurs only negligible cost, is then used for all the other frequencies needed for the synthesis. While more difficult model reduction problems such as those arising in semiconductor device simulation require repeating this process at several reference frequencies across the spectral

bandwidth of interest, our experience has shown the time evolution of the electromagnetic fields after a current shut-off to be a very benign problem for which one reference frequency suffices. After obtaining frequency-domain approximations at the receiver locations for all required frequencies in this way, the associated transients are synthesized using a fast Hankel transform (cf. (Newman et al., 1986)). The resulting algorithm thus has as its main expense the FE solution at the reference frequency and the Arnoldi process to construct the Krylov space. Since each Arnoldi step requires the solution of a linear system with the coefficient matrix associated with the reference frequency problem, we generate a sparse LU factorization of this matrix, which we found feasible for problem sizes of up to around 250,000 using the PARDISO software of Schenk and Gärtner (2004). For much larger problems the linear systems can instead be solved iteratively. Our computational experiments demonstrate that the proposed method can, as an example, compute transients at several receiver locations based on a discretization with 100,000 degrees of freedom in roughly 5 minutes wall clock time on current desktop hardware.

We note that solutions to such multiple-frequency partial-field problems have been published by Wagner et al. (2003) in the context of an acoustic fluid-structure interaction problem.

Without loss of generality, we restrict our 2D and 3D numerical experiments to a simple 1D conductivity structure. For such conductivity models, analytical solutions are readily available.

We complete the model studies with a problem set arising from marine controlled source electromagnetic applications as described by Edwards (2005).

3 Theoretical background

The behaviour of the transient electromagnetic fields after a source current shut-off is described by an initial boundary value problem for Maxwell's equations in quasi-static approximation

$$\nabla \times \boldsymbol{h} - \sigma \boldsymbol{e} = \boldsymbol{j}^e, \tag{1a}$$

$$\partial_t \boldsymbol{b} + \nabla \times \boldsymbol{e} = \boldsymbol{0}, \tag{1b}$$

$$\nabla \cdot \boldsymbol{b} = 0, \tag{1c}$$

where we denote by $\boldsymbol{e}(\boldsymbol{r}, t)$ the electric field, $\boldsymbol{h}(\boldsymbol{r}, t)$ the magnetic field, $\boldsymbol{b}(\boldsymbol{r}, t) = \mu \boldsymbol{h}(\boldsymbol{r}, t)$ the magnetic flux density, $\mu(\boldsymbol{r})$ is the magnetic permeability, and $\boldsymbol{j}^e(\boldsymbol{r}, t)$ external source current density, respectively. The spatial variable $\boldsymbol{r}$ is restricted to a computational domain $\Omega \subset \mathbb{R}^3$ bounded by an artificial boundary Γ, along which appropriate boundary conditions on the tangential components of the fields are imposed,

whereas $t \in \mathbb{R}$. The forcing results from a known stationary transmitter source with a driving current which is shut off at time $t = 0$, and hence of the form

$$\boldsymbol{j}^e(\boldsymbol{r}, t) = \boldsymbol{q}(\boldsymbol{r})H(-t) \tag{2}$$

with the vector field $\boldsymbol{q}$ denoting the spatial current pattern and H the Heaviside step function. The Earth's electrical conductivity is denoted by the parameter $\sigma(\boldsymbol{r})$. We assume negligible coupling between displacement currents and induced magnetic fields, which is valid at late times after current shut-off. After eliminating $\boldsymbol{b}$ from (1) we obtain the second order partial differential equation

$$\nabla\times(\mu^{-1}\nabla\times\boldsymbol{e}) + \partial_t\,\sigma\boldsymbol{e} = -\partial_t\,\boldsymbol{j}^e \quad \text{in } \Omega \tag{3a}$$

for the electric field, which we complete with the perfect conductor boundary condition

$$\boldsymbol{n}\times\boldsymbol{e} = 0 \quad \text{on } \Gamma, \tag{3b}$$

at the outer walls of the model. It should be noted that by doing so, the electric fields at the boundary Γ no longer depend on time t. Switching to the frequency domain, we introduce the Fourier transform pair

$$\boldsymbol{e}(t) = \frac{1}{2\pi}\int_{-\infty}^{\infty} \boldsymbol{E}(\omega)\, e^{\,i\omega t}\, d\omega =: (\mathscr{F}^{-1}\boldsymbol{E})(t), \tag{4}$$

$$\boldsymbol{E}(\omega) = \int_{-\infty}^{\infty} \boldsymbol{e}(t)\, e^{\,-i\omega t}\, dt = (\mathscr{F}\boldsymbol{e})(\omega), \tag{5}$$

ω denoting angular frequency. The representation (4) can be interpreted as a synthesis of the electric field $\boldsymbol{e}(t)$ from weighted time-harmonic electric partial waves $\boldsymbol{E}(\omega)$, whereas (5) determines the frequency content of the time-dependent electric field $\boldsymbol{e}$. We thus obtain the transformed version

$$\nabla\times(\mu^{-1}\nabla\times\boldsymbol{E}) + i\omega\sigma\boldsymbol{E} = \boldsymbol{q} \qquad \text{in } \Omega, \tag{6a}$$

$$\boldsymbol{n}\times\boldsymbol{E} = 0 \qquad \text{on } \Gamma, \tag{6b}$$

of (3a) and (3b) provided that solutions exist for all frequencies $\omega \in \mathbb{R}$. In (6a) we have used the fact that, for the time-dependence $e^{\,i\omega t}$ differentiation with respect to the time variable t becomes multiplication with $i\omega$ in the transformed equations as well as the formal identity $\mathscr{F}(H(-t)) = -1/(i\omega)$, which recflects the fact that the step response due to a current shut-off in a transmitter source is related to an impulsive source by a time derivative $\partial_t H(t) = \delta(t)$, where δ denotes the Dirac impulse, and $\mathscr{F}(\delta) \equiv 1$.

For a given number of discrete frequencies, the Fourier representation (4) of the solution $\boldsymbol{e}$ of (3) can be utilized to construct an approximate solution in the time domain by a Fourier synthesis. Causality of the field in the time domain allows for a representation of the solution in terms of a sine or cosine transform of the real or imaginary part of $\boldsymbol{E}$, resp. (Newman et al., 1986):

$$\boldsymbol{e}(t) = \frac{2}{\pi} \int_0^\infty \mathrm{Re}(\boldsymbol{E}) \, \frac{\sin \omega t}{\omega} \, d\omega = \frac{2}{\pi} \int_0^\infty \mathrm{Im}(\boldsymbol{E}) \, \frac{\cos \omega t}{\omega} \, d\omega. \tag{7}$$

In practice, the infinite range of integration is restricted to a finite range and the resulting integrals are evaluated by a Fast Hankel Transform (Johansen & Sorensen, 1979). For the problems addressed here, solutions for 80 to 150 frequencies distributed over a broad spectral bandwidth with $f \in [10^{-2}, 10^{9}]$ Hz are required to maintain the desired accuracy.

4 Finite element discretization in space

For the solution of boundary value problems in geophysics, especially for geo-electromagnetic applications, finite difference methods have mainly been utilized due to their low implementation effort. However, finite element methods offer many advantages. Using triangular or tetrahedral elements to mesh a computational domain allows for greater flexibility in the parametrization of conductivity structures without the need for staircasing at curved boundaries, such as arise with terrain or sea-floor topography. In addition, there is a mature FE convergence theory for electromagnetic applications (Monk, 2003). Finally, FE methods are much more suitable for adaptive mesh refinement, adding yet further to their efficiency.

For the construction of a FE approximation, we first express the boundary value problem (6) in variational or weak form (Monk, 2003). The weak form requires the equality of both sides of (6a) in the inner product sense only. The $L^2(\Omega)$ inner product of two complex vector fields $\boldsymbol{u}$ and $\boldsymbol{v}$ is defined as

$$(\boldsymbol{u}, \boldsymbol{v}) = \int_\Omega \boldsymbol{u} \cdot \bar{\boldsymbol{v}} \, dV \tag{8}$$

with $\bar{\boldsymbol{v}}$ denoting the complex conjugate of $\boldsymbol{v}$. Taking the inner product of (6a) with the smooth vector field $\boldsymbol{\varphi}$—called the test function—and integrating over Ω, we obtain after an integration by parts

$$\int_\Omega \left[(\mu^{-1} \nabla \times \boldsymbol{E}) \cdot (\nabla \times \bar{\boldsymbol{\varphi}}) + i\omega\sigma \boldsymbol{E} \cdot \bar{\boldsymbol{\varphi}} \right] dV - \int_\Gamma (\boldsymbol{n} \times \bar{\boldsymbol{\varphi}}) \cdot (\mu^{-1} \nabla \times \boldsymbol{E}) \, dA = \int_\Omega \boldsymbol{q} \cdot \bar{\boldsymbol{\varphi}} \, dV. \tag{9}$$

On Γ, the perfect conductor boundary condition (6b) gives no information about $(\mu^{-1}\nabla\times\boldsymbol{E})$, so we eliminate this integral by choosing $\boldsymbol{\varphi}$ such that $\boldsymbol{n}\times\boldsymbol{\varphi}=0$ on Γ.

Introducing the solution space

$$\mathscr{E} := \{\boldsymbol{v}\in\boldsymbol{H}(\mathrm{curl};\Omega) : \boldsymbol{n}\times\boldsymbol{v}=\boldsymbol{0} \text{ on } \Gamma\},$$

in terms of the Sobolev space $\boldsymbol{H}(\mathrm{curl};\Omega) = \{\boldsymbol{v}\in L^2(\Omega)^3 : \nabla\times\boldsymbol{v}\in L^2(\Omega)^3\}$, the weak form of the boundary value problem finally reads

$$\begin{aligned}&\textit{Find } \boldsymbol{E}\in\mathscr{E} \textit{ such that}\\ &\int_\Omega \left[(\mu^{-1}\nabla\times\boldsymbol{E})\cdot\nabla\times\bar{\boldsymbol{v}} + i\omega\sigma\boldsymbol{E}\cdot\bar{\boldsymbol{v}}\right] dV = \int_\Omega \boldsymbol{q}\cdot\bar{\boldsymbol{v}}\,dV \qquad \textit{for all } \boldsymbol{v}\in\mathscr{E}.\end{aligned} \tag{10}$$

Due to the homogeneous boundary condition (6b) the trial and test functions can be chosen from the same space $\mathscr{E}$.

To construct a FE solution of the boundary value problem (6) the domain Ω is partitioned into simple geometrical subdomains, e.g. triangles for two-dimensional or tetrahedra for three-dimensional problems, such that

$$\Omega = \bigcup_{e=1}^{N_e} \Omega_e. \tag{11}$$

The infinite-dimensional function space $\mathscr{E}$ is approximated by a finite dimensional function space $\mathscr{E}^h\subset\mathscr{E}$ of elementwise polynomial functions satisfying the homogeneous boundary condition (6b).

The approximate electric field $\boldsymbol{E}^h\approx\boldsymbol{E}$ is defined as the solution of the discrete variational problem obtained by replacing $\mathscr{E}$ by $\mathscr{E}^h$ in (10) (cf. Monk (2003)).

To obtain the matrix form of (10), we express $\boldsymbol{E}^h$ as a linear combination of basis functions $\{\boldsymbol{\varphi}_i\}_{i=1}^N$ of $\mathscr{E}^h$, i.e.

$$\boldsymbol{E}(\boldsymbol{r}) = \sum_{i=1}^{N} E_i\,\boldsymbol{\varphi}_i(\boldsymbol{r}). \tag{12}$$

Testing against all functions in $\mathscr{E}^h$ is equivalent to testing against all basis functions $\boldsymbol{\varphi}_j, j=1,\ldots,N$. Taking the j-th basis function as the test function and inserting (12) into (10) yields the j-th row of a linear system of equations

$$(\mathbf{K}+i\omega\mathbf{M})\,\mathbf{u} = \mathbf{f} \tag{13}$$

for the unknown coefficients $E_i = [\mathbf{u}]_i$, $i = 1, \ldots, N$, where

$$[\mathbf{K}]_{j,i} = \int_\Omega (\mu^{-1} \nabla \times \boldsymbol{\varphi}_i) \cdot \nabla \times \bar{\boldsymbol{\varphi}}_j \, dV, \tag{14}$$

$$[\mathbf{M}]_{j,i} = \int_\Omega \sigma \boldsymbol{\varphi}_i \cdot \bar{\boldsymbol{\varphi}}_j \, dV, \tag{15}$$

$$[\mathbf{f}]_j = \int_\Omega \boldsymbol{q} \cdot \bar{\boldsymbol{\varphi}}_j \, dV. \tag{16}$$

The matrices $\mathbf{K}$ and $\mathbf{M}$, known as *stiffness* and *mass matrix*, respectively, in finite element parlance, are large and sparse and, since μ and σ are real-valued quantities in the problem under consideration, consist of real entries.

For a given source vector $\mathbf{f}$ determined by the right-hand side of (6a), the solution vector $\mathbf{u} \in \mathbb{C}^N$ yields the approximation $\boldsymbol{E}^h$ of the electric field $\boldsymbol{E}$ we wish to determine.

5 Model reduction

Our goal is the efficient computation of the finite element approximation $\boldsymbol{E}^h$ in a subset of the computational domain Ω. To this end, we fix a subset of $p \ll N$ components of the solution vetor $\mathbf{u}$ to be computed. These correspond to p coefficients in the finite element basis expansion (12), and thus, in the lowest-order Nédélec spaces we have employed, directly to components of the approximate electric field $\boldsymbol{E}^h$ in the direction of selected edges of the mesh. We introduce the discrete extension operator $\mathbf{E} \in \mathbb{R}^{N \times p}$ defined as

$$[\mathbf{E}_{i,j}] = \begin{cases} 1, & \text{if the } j\text{-th coefficient to be computed has global index } i, \\ 0, & \text{otherwise.} \end{cases}$$

Multiplication of a coefficient vector $\mathbf{v} \in \mathbb{C}^N$ with respect to the finite element basis by $\mathbf{E}^\top$ then extracts the p desired components, yielding the reduced vector $\mathbf{E}^\top \mathbf{v} \in \mathbb{C}^p$ containing the field values at the points of interest.

For the solution $\mathbf{u}$, this reduced vector, as a function of frequency, thus takes the form

$$\mathbf{t} = \mathbf{t}(\omega) = \mathbf{E}^\top (\mathbf{K} + i\omega \mathbf{M})^{-1} \mathbf{f} \in \mathbb{C}^p. \tag{17}$$

The vector-valued function $\mathbf{t}(\omega)$ in equation (17) assigns, for each frequency ω, the output values of interest to the source (input) data represented by the right-hand-side vector $\mathbf{f}$.

Computing $\mathbf{t}(\omega)$ for a given number of frequencies $\omega_j \in [\omega_{\min}, \omega_{\max}],\ j = 1, \ldots, N_f$, by solving N_f full systems and then extracting the p desired components from each is computationally expensive, if not prohibitive, for large N. This situation is similar to that of linear systems theory, where the function $\mathbf{t}$ is known as a *transfer function* and the objective is to approximate $\mathbf{t}$ based on a model with significantly fewer degrees of freedom than N, hence the term *model reduction*.

To employ model reduction techniques, we proceed by fixing a reference frequency ω_0 and rewriting (17) as

$$\mathbf{t} = \mathbf{t}(s) = \mathbf{E}^\top [\mathbf{A}_0 - s\mathbf{M}]^{-1}\mathbf{f}, \qquad \mathbf{A}_0 := \mathbf{K} + i\omega_0\mathbf{M}, \tag{18}$$

where we have also introduced the (purely imaginary) *shift parameter* $s = s(\omega) := i(\omega_0 - \omega)$. Setting further $\mathbf{L} := \mathbf{E} \in \mathbb{R}^{N\times p}$, $\mathbf{r} := \mathbf{A}_0^{-1}\mathbf{f} \in \mathbb{C}^N$, and $\mathbf{A} := \mathbf{A}_0^{-1}\mathbf{M} \in \mathbb{C}^{N\times N}$, the transfer function becomes

$$\mathbf{t}(s) = \mathbf{L}^\top (\mathbf{I} - s\mathbf{A})^{-1}\mathbf{r}. \tag{19}$$

The transfer function is a rational function of s (and hence of ω), and a large class of model reduction methods consist of finding lower order rational approximations to $\mathbf{t}(s)$. The method we shall propose constructs a Padé-type approximation with respect to the expansion point ω_0, i.e., $s = 0$. The standard approach (Gragg & Lindquist, 1983; Freund, 2003; Antoulas, 2005) for computing such approximations in a numerically stable way is by Krylov subspace projection. For simplicity, we shall consider an orthogonal projection onto a Krylov space based on Arnoldi's method.

Given a matrix $\mathbf{C}$ and a nonzero initial vector $\mathbf{x}$, the Arnoldi process successively generates orthonormal basis vectors of the nested sequence

$$\mathscr{K}_m(\mathbf{C}, \mathbf{x}) := \operatorname{span}\{\mathbf{x}, \mathbf{C}\mathbf{x}, \ldots, \mathbf{C}^{m-1}\mathbf{x}\}, \qquad m = 1, 2, \ldots$$

of *Krylov spaces* generated by $\mathbf{C}$ and $\mathbf{x}$, which are subspaces of dimension m up until m reaches a unique index L, called the grade of $\mathbf{C}$ with respect to $\mathbf{x}$, after which these spaces become stationary. In particular, choosing $\mathbf{C} = \mathbf{A}$ and $\mathbf{x} = \mathbf{r}$, m steps of the Arnoldi process result in the *Arnoldi decomposition*

$$\mathbf{A}\mathbf{V}_m = \mathbf{V}_m\mathbf{H}_m + \eta_{m+1,m}\mathbf{v}_{m+1}\mathbf{e}_m^\top, \qquad \mathbf{r} = \beta\mathbf{v}_1, \tag{20}$$

in which the columns of $\mathbf{V}_m \in \mathbb{C}^{N\times m}$ form an orthonormal basis of $\mathscr{K}_m(\mathbf{A}, \mathbf{r})$, $\mathbf{H}_m \in \mathbb{C}^{m\times m}$ is an unreduced upper Hessenberg matrix, $\mathbf{v}_{m+1}$ is a unit vector orthogonal to $\mathscr{K}_m(\mathbf{A}, \mathbf{r})$ and $\mathbf{e}_m$ denotes the m-th unit coordinate vector in $\mathbb{C}^m$. In particular, we have the relation $\mathbf{H}_m = \mathbf{V}_m^\top\mathbf{A}\mathbf{V}_m$. Using the orthonormal basis $\mathbf{V}_m$, we may project the vector $\mathbf{r}$ as well as the columns of $\mathbf{L}$ in (19) orthogonally onto

$\mathscr{K}_m(\mathbf{A}.\mathbf{r})$ and replace the matrix $\mathbf{I} - s\mathbf{A}$ by its compression $\mathbf{V}_m^\top(\mathbf{I} - s\mathbf{A})\mathbf{V}_m$ onto $\mathscr{K}_m(\mathbf{A}, \mathbf{r})$, yielding the approximate transfer function

$$\mathbf{t}_m(s) := (\mathbf{V}_m^\top \mathbf{L})^\top [\mathbf{V}_m^\top (\mathbf{I} - s\mathbf{A})\mathbf{V}_m]^{-1} (\mathbf{V}_m^\top \mathbf{r}) = \mathbf{L}_m^\top (\mathbf{I}_m - s\mathbf{H}_m)^{-1} \beta \mathbf{e}_1,$$

where we have set $\mathbf{L}_m := \mathbf{V}_m^\top \mathbf{L}$ and used the properties of the quantities in (20) stated above.
Given the task of evaluating the transfer function (17) for N_f frequencies $\omega_j \in [\omega_{\min}, \omega_{\max}]$, our model reduction approach now proceeds as detailed in Algorithm 1.

Algorithm 1: Model reduction for TEM in the frequency domain.

Select a reference frequency ω_0

Set $\mathbf{A}_0 := \mathbf{K} + i\omega_0\mathbf{M}$, $\mathbf{A} := \mathbf{A}_0^{-1}\mathbf{M}$ and $\mathbf{r} := \mathbf{A}_0^{-1}\mathbf{f}$

Perform m steps of the Arnoldi process yielding decomposition (20)

for $j = 1, 2, \ldots, N_f$ **do**

  Set $s_j := \omega - \omega_j$

  Evaluate approximate transfer function $\mathbf{t}_m(s_j)$

Note that computations with large system matrices and vectors with the full number N of degrees of freedom are required only in the Arnoldi process, after which the loop across the target frequencies takes place in a subspace of much smaller dimension $m \ll N$. As a consequence, the work required in the latter is almost negligible in comparison. The most expensive step of the Arnoldi process is the matrix-vector multiplication with the matrix $\mathbf{A}_0$. Currently, we compute an LU factorization of $\mathbf{A}_0$ in a preprocessing step and use the factors to compute the product with two triangular solves.
We note that current Krylov subspace-based model reduction techniques employ more refined subspace generation techniques, in particular block algorithms to take into account all columns of $\mathbf{L}$ in the subspace generation as well as two-sided Lanczos (Feldmann & Freund, 1994) and Arnoldi (Antoulas, 2005) methods to increase the approximation order of the transfer function. We intend to evaluate these refinements for the present TEM application in future work. However, we have been able to obtain surprisingly good results usung this very basic method. A further enhancement is replacing the LU factorization of $\mathbf{A}_0$ with an inner iteration once the former is no longer feasible due to memory constraints.

6 Numerical examples

To validate of our approach we consider as a model problem a vertical magnetic dipole over a layered halfspace. The reason for this choice is twofold: First, an analytical solution is available for direct comparison with the numerical approximation. Second, the huge conductivity contrast due to including the air layer in the computational domain presents a severe challenge for realistic simulations. Besides comparison with the analytical solution we also check our solution against one obtained by the Spectral Lanczos Decomposition Method.

The FE discretization was carried out using the Electromagnetics Module of the COMSOL Multiphysics package, where we have used second order Lagrange elements on triangles in the 2D calculations and second-order Nédélec elements on tetrahedra for 3D. The sparse LU decomposition required in our algorithm as well as the triangular solves based on this decomposition are performed using the PARDISO software of Schenk and Gärtner (2004, 2006). Our own code is written in MATLAB, from where the appropriate COMSOL and PARDISO components are called. All computations were carried out on a 3.0 GHz Intel Xeon 5160 with 16 GB RAM running Suse Linux 10.1.

6.1 The 2D axisymmetric case

We begin our numerical experiments with a 2D axisymmetric study in order to demonstrate the interplay of the three main discretization parameters: mesh resolution, size of the computational domain and the dimension of the Krylov subspace used for the frequency sweep. The FE discretization contains two sources of error: one arising from the usual dependence of the error on the mesh width, i.e., resolution, the other arising from imposing a non-exact boundary condition at the non-symmetry boundaries. As we are modelling a diffusion process, the error due to the boundary condition decreases rapidly with the size of the computational domain. An efficient discretization should balance these two types of error, i.e., the domain size and mesh width should be chosen such that these two errors are of comparable magnitude. The third relevant parameter, the dimension of the Krylov space, determines the size of the reduced model, and should be large enough to provide a sufficiently good approximation of the transfer function so that the time-domain solution is sufficiently accurate.

We consider the fields of a vertical magnetic dipole over an axially-symmetric conductivity structure. The dipole is aligned with the z-axis of a cylindrical coordinate system and is approximated by a finite circular coil with a radius of 5 m. Due to the symmetry of the problem, we may restrict the computational

domain to the $r-z$-plane of the coordinate system thus resulting in a purely 2D problem.

The conductivity structure we consider consists of a 30 m thick 30 $\Omega\cdot\mathrm{m}$ layer at a depth of 100 m embedded in a uniform halfspace of 100 $\Omega\cdot\mathrm{m}$ (cf. Fig. 1). For the FE discretization, second-order (node based) Lagrange elements were used to compute the tangential component of the electric field in the frequency domain. The reference frequency was 1000 Hz. For the analytical reference solution we employ the quasistatic approximation of Ward and Hohmann (1988), from which we obtain the time-domain solution via a Hankel transform. Note that the quasistatic approximation deteriorates at high frequencies. The numerical results obtained by the Arnoldi model reduction method are compared with the analytical 1D model results.

To demonstrate the influence of the computational domain size and the number of triangles involved, we choose different geometries. Three horizontal model sizes of $\pm$600 (model 1), $\pm$1200 (model 2), and $\pm$2400 meters (model 3) are considered. Fig. 2 shows the discretized conductivity region for these three domain sizes. The small elements in the vicinity of the transmitter coil result from three successive adaptive mesh refinement steps of COMSOL's default *a posteriori* error estimator, in which the mesh refinement is performed by remeshing. The FE spaces based on these three meshes contained 11,227 (model 1), 7,850 (model 2) and 29,358 (model 3) degrees of freedom, respectively.

Furthermore, by specifying the maximum number of new triangles generated in each adaptive cycle, we introduce a rough upper bound of the final mesh resolution.

The resulting transfer functions and transient electric fields on the air-earth interface at 100 meters distance from the dipole location are depicted in Fig. 3. For a Krylov subspace of dimension $m = 60$ we observe a substantial error in the high frequencies, which is significantly reduced in the case $m = 200$. However, this error does not affect the transient field at the corresponding short times (cf. Fig. 3, right), where the agreement with the analytical solution is equally good in all cases. The reason for this is that, when the Hankel transform is carried out to synthesize the transient field, the high-frequency values of the transfer function are damped in such a way that these errors have little effect on the solution. We have not plotted relative errors here, since high frequencies are near the limits of validity of the analytical reference solution.

We observe a strong dependence of the synthesized late time solution on the distance of the outer boundary, where the perfect conductor boundary condition is imposed, enforcing a vanishing tangential component of the electric field there. Since, for each frequency, we are solving a damped wave equation in which damping increases with frequency (at fixed conductivity), the solutions at higher frequencies

decay faster towards the outer boundary. Therefore, the effect of error due to the inexact boundary condition is greatest at the lowest frequency. In the time domain, this is observed at late times, when all but the low frequency components have decayed.

The non-exact boundary condition leads to consistency errors in the corresponding low frequency response for which the problem is originally formulated in terms of the matrix $\mathbf{A}_0$. Adjusting the outer boundaries improves the solution significantly. On the other hand, by restricting the total number of triangles within the discretized region, a coarser mesh in regions where steep changes in the solutions occur must be expected. To counteract this tendency, more Arnoldi iterations steps are necessary to obtain a satisfactory approximation of the high frequency part of the solution.

On the left hand side in Fig. 4, we display the relative error in the transient electric field at a distance of 100 m from the source. For model 1 the error

$$\frac{e_{an}(t) - e_m(t)}{e_{an}(t)} \cdot 100\%$$

with $e_{an}(t)$ denoting the analytical solution and $e_m(t)$ the solution after m Arnoldi steps, is dominated at late times by the effect of the boundary condition, and increasing the Krylov subspace dimension from $m = 60$ to $m = 200$ does not result in an improvement. For models 2 and 3, by contrast, a considerable improvement can be observed for the larger Krylov subspace, particularly for late times in the 2400 m case. The convergence with increasing m, measured in terms of the relative error $||e_{an}(t) - e_m(t)||/||e_{an}||$, where $||\cdot||$ denotes the Euclidean norm of the transient at the receiver point for 31 discrete time values spaced logarithmically in $[10^{-6}, 10^{-3}]$, indicates that the finer mesh resolution in the case of model 1 needs substantially fewer Arnoldi iterations than the larger models 2 and 3.

Finally, the computing time is dominated by the Arnoldi process. Once the Arnoldi basis of the Krylov space has been computed, the sweep over the frequencies adds only negligible work. Computing time for the sparse LU decomposition can also be neglected, which is typical for 2D problems.

6.2 The full 3D case

For the numerical experiments in 3D we use vector (Nédélec) finite elements with quadratic basis functions. The FE approximation of the electric field is therefore associated with the edges of the tetrahedral elements. The vertical magnetic transmitter dipole source is approximated by a square loop of 10 m edge length located in the plane defined by $z = 0$. The electric current flowing inside the loop is associated with edge currents attributed to the edges of those tetrahedral elements which coincide with the loop

position. The receiver forms a square loop of 4 m edge length. It is located at $z = 0$ m, 100 m away from the center of the transmitter loop. Therefore, the y-components of the electric fields are associated with the two edges perpendicular to the x-direction at $x = 98$ and $x = 102$ m, respectively. The x-components of the electric field can be obtained at $y = -2$ and $y = 2$ m and $x = 100$ m. With these four components we can numerically approximate the curl of electric fields yielding an estimate of the voltage induced within the loop,

$$\partial_t B_z = \partial_y E_x - \partial_x E_y. \tag{21}$$

Fig. 5 shows a horizontal cross-section of the 3D tetrahedral mesh at $z = 0$. It illustrates the distribution of the tetrahedral finite elements after adaptive mesh refinement. Small elements occur near the transmitter coil, i.e., where the solution exhibits large gradients. The entire 3D mesh consists of 12,218 tetrahedra, which corresponds to 79,844 degrees of freedom. We note that second-order Nédélec elements contain six degrees of freedom per tetrahedron. The finite difference grid used with the SLDM experiments is depicted in Fig. 6. Due to the nature of the tensor product grids used there, unnecessarily fine grid cells occur at the outer boundaries of the discretized region.

Both meshes lead to solutions of comparable accuracy. However, compared with a solution vector of 108,000 entries for the SLDM approach, the total number of degrees of freedom is only $79,844$ for the adaptively refined finite element discretization.

Fig. 7(a) shows the real part of the transfer function at $x = 98$ m for Krylov subspaces of dimension $m = 60$ and $m = 200$. As in the 2D example, we observe that the approximation begins to deteriorate at roughly a frequency of 10^6 Hz. We attribute this to the resolution of the finite element mesh, which is less in comparison to the 2D case. Again as in the 2D example, we observe in Fig. 7(b) that the Hankel transform in the synthesis of the time domain solution effectively damps out the errors in the transfer function in the high frequencies, resulting in good agreement of the transient electrig field with the analytical solution at $x = 98$ m for a Krylov subspace dimension of $m = 200$. The plots in Figure 7(c) show that increasing the size of the Krylov space resulted in a clear improvement at early times. By contrast, we attribute any remaining error at late simulation times to the proximity of the boundary of the computational domain, where the perfect conductor boundary condition is imposed. This discretization feature cannot be compensated by a larger Krylov space. Fig. 7(d) shows a similar behavior of cpu time against the number of Arnoldi steps. The convergence is, however, less steep, what we attribute to the lower mesh resolution in the 3D case.

We state explicitly, that the computing time required to compute the required frequency domain solutions

by the Arnoldi based model reduction technique is essentially negligible (Fig. 8) in comparison with the Arnoldi process itself.

Fig. 9 shows a comparison of the transient electric field at $x = 98$ m computed with our Arnoldi-based model reduction approach with that produced by a competing algorithm for time-dependent TEM-simulation, the Spectral Lanczos Decomposition Method (SLDM) of Druskin and Knizhnerman (1988). We observe good agreement of both approximations with the analytic solution. Comparing the relative errors of both methods, we observe a substantially larger error of the SLDM approximation especially at early times.

Finally, Figure 10 shows the value and relative errors of $\partial_t b_z$ at $x = 100$ m obtained by computing the curl of the electric field approximation (cf. Eq. 21). Again we observe the large relative error of the SLDM approximation at early simulation times.

This comparison suggests that the model reduction method seems to result in approximations which are more accurate at early times of the transient simulation. We note that, for practical purposes, it is this early phase where accuracy is most needed, as measurement data tends to become more uncertain later in the process. Moreover, when considering the more important inverse TEM problem, the measured fields in the early phase of the process are most emphasized.

6.3 Marine EM simulation

We conclude our numerical experiments with a model situation which is typical for the emerging sector of marine controlled source electromagnetic applications. We consider an electric dipole source as a transmitter which is laid out at the seafloor. A set of receivers measure the inline electric field components after source current turn-on (Fig. 11).

For the numerical experiments we make use of a similar model setup. The source is now an electric dipole which can be associated with an edge current flowing along an edge of a tetrahedron. The electric inline components can be assessed in the same manner as in the former 3D experiment.

As an example, we consider the case of a small resistive body embedded in a good conducting environment. For late times after current turn-on, the response of the body is comparable to the case of DC resistivity experiments. We observe an increase of late time inline electric fields particularly when the body is in the most sensitive region of the transmitter-receiver-system (Fig. 12). For details on sensitivity distribution for DC resistivity applications, see (Spitzer, 1998).

As an additional feature of our method, we note that identical results are obtained when transmitter and

receiver positions are exchanged, i.e., the reciprocity relation due to the symmetry of the chosen dipole configuration is preserved.

7 Conclusions

We have developed an effective algorithm for simulating the electromagnetic field of a transient dipole source. Using a Krylov subspace projection technique, the system of equations arising from the FE discretization of the time-harmonic equation is projected onto a low-dimensional subspace. The resulting system can be solved for a wide range of frequencies with only moderate computational effort. In this way, computing transients using a Fourier transform becomes feasible.

Numerical comparisons for a model problem have shown the model reduction method to be more accurate for early simulation times, which is the more relevant phase of the process in practical applications and inversion calculations.

We also emphasize that the FE discretization provides more flexibility with regard to the parametrization of conductivity varations, topography, dipping layers and bathymetry. Adaptive mesh refinement, which is essential for strongly varying gradients in the fields, as well as *a posteriori* error approximation, are also much more easily handled in a finite element context.

A further advantage of the frequency domain calculations is that no initial field data are required, as is the case for time domain simulation schemes.

Finally, we mention some possible improvements of the model reduction frequency domain method: we have chosen the Arnoldi process for generating the Krylov subspace basis, and used a one-sided approximation to approximate the transfer function. A better approximation with a smaller Krylov space can be achieved using two-sided projections and more efficient Krylov subspace basis generation based on the unsymmetric block Lanczos process. In addition, for very large 3D calculations the time and memory cost for computing the LU decomposition of the matrix $\mathbf{A}_0$ can become excessive, so that multigrid methods recently developed specifically for the curl-curl operator could replace the linear system solves with $\mathbf{A}_0$ required at each step of the Krylov subspace generation. We will investigate these enhancements in future work.

Acknowledgments

Part of this study has been funded by the Deutsche Forschungsgemeinschaft under Sp 356/9-1. The authors thank Roland Martin (Univ. of Cologne) for kindly providing the SLDM numerical checks.

References

Anderson, W. L. (1979). Numerical integration of related Hankel transforms of orders 0 and 1 by adaptive digital filtering. *Geophysics*, *44*, 1287-1305.

Antoulas, A. C. (2005). *Approximation of large-scale dynamical systems*. Philadelphia, PA: SIAM Publications.

Commer, M., & Newman, G. (2004). A parallel finite-difference approach for 3D transient electromagnetic modeling with galvanic sources. *Geophysics*, *69*(5), 1192-1202.

Druskin, V. L., & Knizhnerman, L. A. (1988). Spectral differential-difference method for numeric solution of three-dimensional nonstationary problems of electric prospecting. *Izvestiya, Earth Physics*, *24*, 641-648.

Edwards, N. (2005). Marine controlled source electromagnetics: Principles, methodologies, future commercial applications. *Surveys in Geophysics*, *26*, 675-700.

Everett, M., & Edwards, R. (1993). Transient Marine Electromagnetics - the 2.5-D forward problem. *Geophysical Journal International*, *113*(3), 545-561.

Feldmann, P., & Freund, R. W. (1994). Efficient linear circuit analysis by Padé approximation via the Lanczos process. In *Proceedings of EURO-DAC '94 with EURO-VHDL '94, Grenoble, France* (pp. 170–175). Los Alamitos, CA: IEEE Computer Society Press.

Freund, R. W. (2003). Model reduction methods based on Krylov subspaces. *Acta Numerica*, *12*, 267–319.

Goldman, M. M., & Stoyer, C. H. (1983). Finite-difference calculations of the transient field of an axially symmetric earth for vertical magnetic dipole excitation. *Geophysics*, *48*, 953-963.

Gragg, W. B., & Lindquist, A. (1983). On the partial realization problem. *Linear Algebra and its Applications*, *50*, 277–319.

Jin, J., Zunoubi, M., Donepudi, K. C., & Chew, W. C. (1999). Frequency-domain and time-domain finite-element solution of Maxwell's equations using spectral Lanczos decomposition method. *Comput. Meth. Appl. Mech. Engrg.*(169), 279-296.

Johansen, H. K., & Sorensen, K. (1979). Fast Hankel Transforms. *Geophysical Prospecting*, *27*, 876-901.

Mitsuhata, Y. (2000). 2-D electromagnetic modeling by finite-element method with a dipole source and topography. *Geophysics*, *65*(2), 465-475.

Monk, P. (2003). *Finite element methods for Maxwell's equations*. New York: Oxford University Press.

Newman, G. A., Hohmann, G. W., & Anderson, W. L. (1986). Transient electromagnetic response of a three-dimensional body in a layered earth. *Geophysics*, *51*, 1608-1627.

Oristaglio, M. L., & Hohmann, G. W. (1984). Diffusion of electromagnetic fields into a two-dimensional earth: A finite-difference approach. *Geophysics*, *49*, 870-894.

Schenk, O., & Gärtner, K. (2004). Solving unsymmetric sparse systems of linear equations with PARDISO. *Journal of Future Generation Computer Systems*, *20*(3), 475–487.

Schenk, O., & Gärtner, K. (2006). On fast factorization pivoting methods for symmetric indefinite systems. *Elec. Trans. Numer. Anal.*, *23*, 158–179.

Spitzer, K. (1998). The three-dimensional DC sensitivity for surface and subsurface sources. *Geophysical Journal International*, *134*, 736-746.

Sugeng, F., Raiche, A., & Rijo, L. (1993). Comparing the time-domain EM response of 2-D and elongated 3-D conductors excited by a rectangular loop source. *Journal of Geomagnetism and Geoelectricity*, *45*(9), 873-885.

Taflove, A. (1995). *Computational electrodynamics: The finite-difference time-domain method*. Norwood, MA: Artech House.

Wagner, M. M., Pinsky, P. M., Oberai, A. A., & Malhotra, M. (2003). A Krylov subspace projection method for simultaneous solution of Helmholtz problems at multiple frequencies. *Comput. Meth. Appl. Mech. Engrg.*, *192*, 4609–4640.

Wang, T., & Hohmann, G. W. (1993). A finite-difference, time-domain solution for three-dimensional electromagnetic modelling. *Geophysics*, *58*, 797-809.

Ward, S. H., & Hohmann, G. W. (1988). Electromagnetic theory for geophysical applications. In M. Nabighian (Ed.), *Electromagnetic methods in applied geophysics* (chap. 4). Tulsa, Oklahoma, U.S.A.: Soc. Expl. Geoph.

Yee, K. S. (1966). Numerical solution of initial boundary problems involving Maxwell's equations in isotropic media. *IEEE Trans. Ant. Propag.*, *14*, 302-309.

List of Figures

1 Section of the considered conductivity model. The conductive layer is 30 m thick. The dimension of the discretized models 1, 2, and 3 extends to up to ± 600, ±1200, and ±2400 m in the horizontal and vertical directions. In the 2D case, the axis of symmetry is aligned with the z axis. 21

2 Finite element meshes (from left to right) for models 1 (11,227 DOF), model 2 (7,850 DOF), and model 3 (29,359 DOF). 22

3 Transfer function $\mathrm{Re}\, E_\phi(f)$ and transient electric field $e_\phi(t)$ 100 m away from the vertical electric dipole source for model size of 600 m (a, b), 1200 m (c, d), and 2400 m (e, f). 60 and 200 Arnoldi iterations have been considered. 23

4 Relative errors of the transient electric field $e_\phi(t)$ for 60 and 200 Arnoldi iterations with respect to the analytical solution (a, c, e) as well as computing time and convergence of the transient solution for model dimension 600, 1200, and 2400 m (b, d, f). 24

5 Plane view of a section of the 3D finite element mesh (plane at $z = 0$) used for numerical experiments. A total of 500 triangular boundary elements are aligned with the interface at $z = 0$. The full 3D mesh consists of 12,218 tetrahedral elements corresponding to 79,358 DOF. Transmitter and receiver loops are denoted by TX and RX, resp. 25

6 Full extent (a) and section (b) of the finite difference grid ($x - y$-plane, $z = 0$) used for the numerical 3D SLDM experiments. 26

7 Real part of the transfer function at $x = 98$ m (a), transient electric field $e_m(t)$ (b) for $m = 60$ and $m = 200$ Arnoldi iteration steps, relative error of transient electric field (c), as well as computer time and convergence (d). Reference frequency is 1000 Hz. 27

8 Total processor time for the Fourier synthesis of 110 approximated 3D frequency domain solutions against the number of Arnoldi iterations. 28

9 Comparison of transient electric fields (top) and associated relative errors (bottom) for SLDM and Arnoldi solutions at $x = 98$ m. 29

10 Comparison of transient voltage ($\partial_t b_z$, top) and associated relative errors (bottom) for SLDM and Arnoldi solutions at $x = 100$ m. Note that due to the sign reversal of the voltage signal at $t \approx 2 \cdot 10^{-5}$ s, the relative error yields meaningless results and has therefore been omitted from the figure. 30

11 Top view and section of the conductivity structure of the 3D marine model. The seawater layer extends up to 1200 m, the seabottom extends down to -1200 m. We consider transmitter-receiver spacings of 100 and 150 m, respectively. 31

12 Inline transient electric fields $e_x(t)$ for a current turn-on. Transmitter-receiver spacing is assumed to be 100 m (a) and 150 m (b). Indicated are the transients for various positions of the transmitter-receiver-system midpoint x_0 relative to the position of the resistive body. 32

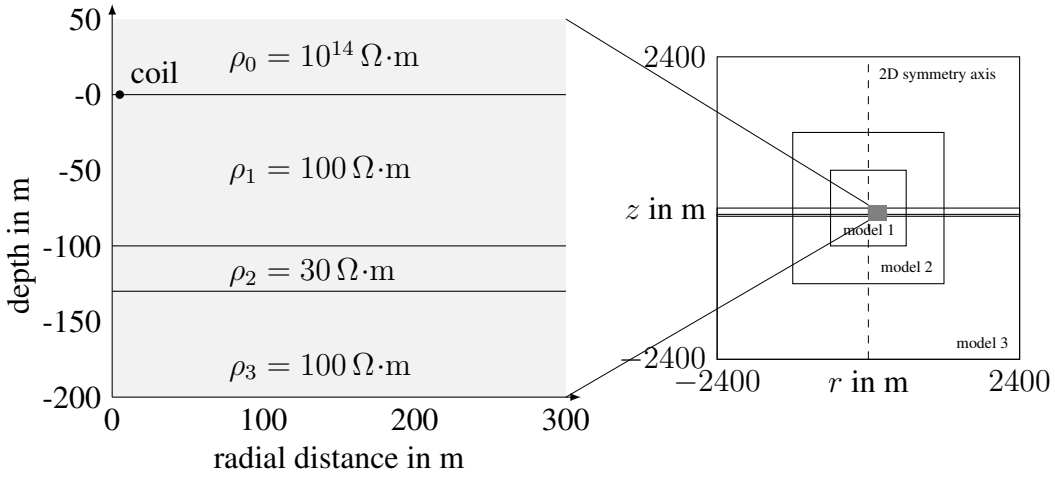

Figure 1: Section of the considered conductivity model. The conductive layer is 30 m thick. The dimension of the discretized models 1, 2, and 3 extends to up to $\pm$ 600, $\pm$1200, and $\pm$2400 m in the horizontal and vertical directions. In the 2D case, the axis of symmetry is aligned with the z axis.

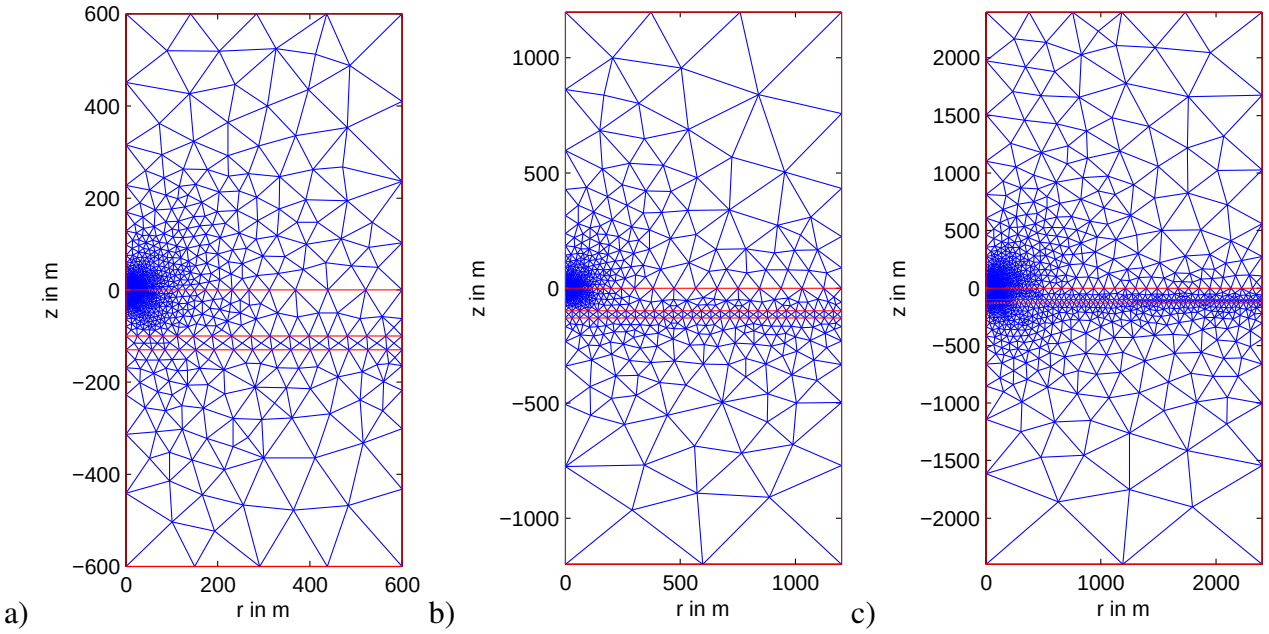

Figure 2: Finite element meshes (from left to right) for models 1 (11,227 DOF), model 2 (7,850 DOF), and model 3 (29,359 DOF).

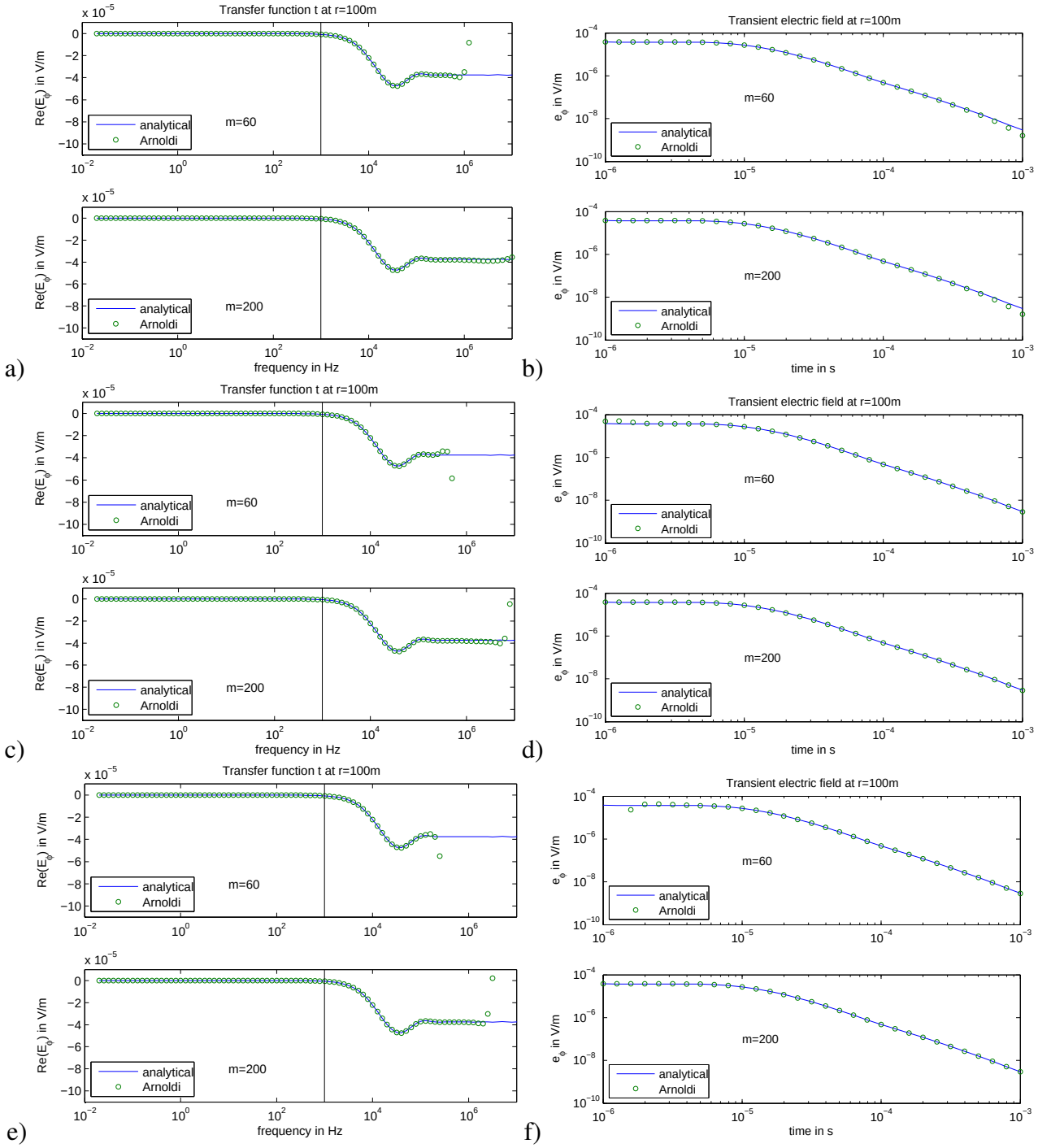

Figure 3: Transfer function $\mathrm{Re}\, E_\phi(f)$ and transient electric field $e_\phi(t)$ 100 m away from the vertical electric dipole source for model size of 600 m (a, b), 1200 m (c, d), and 2400 m (e, f). 60 and 200 Arnoldi iterations have been considered.

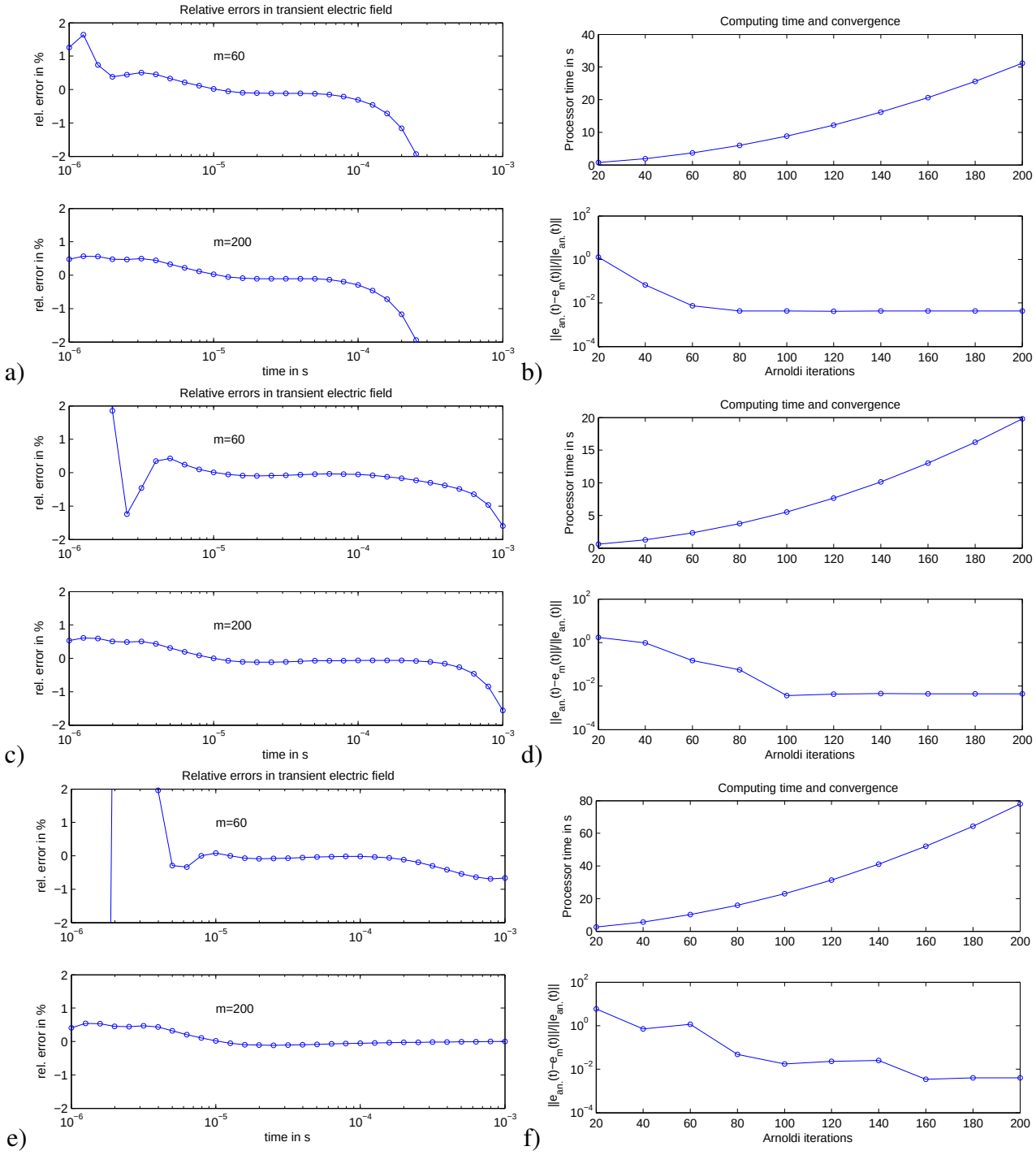

Figure 4: Relative errors of the transient electric field $e_\phi(t)$ for 60 and 200 Arnoldi iterations with respect to the analytical solution (a, c, e) as well as computing time and convergence of the transient solution for model dimension 600, 1200, and 2400 m (b, d, f).

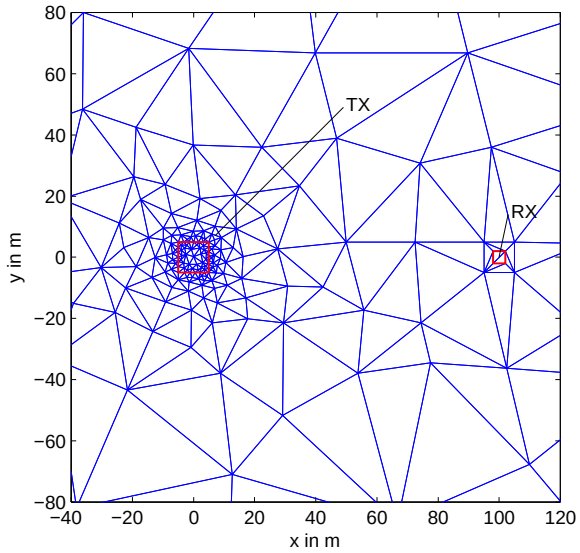

Figure 5: Plane view of a section of the 3D finite element mesh (plane at $z = 0$) used for numerical experiments. A total of 500 triangular boundary elements are aligned with the interface at $z = 0$. The full 3D mesh consists of 12,218 tetrahedral elements corresponding to 79,358 DOF. Transmitter and receiver loops are denoted by TX and RX, resp.

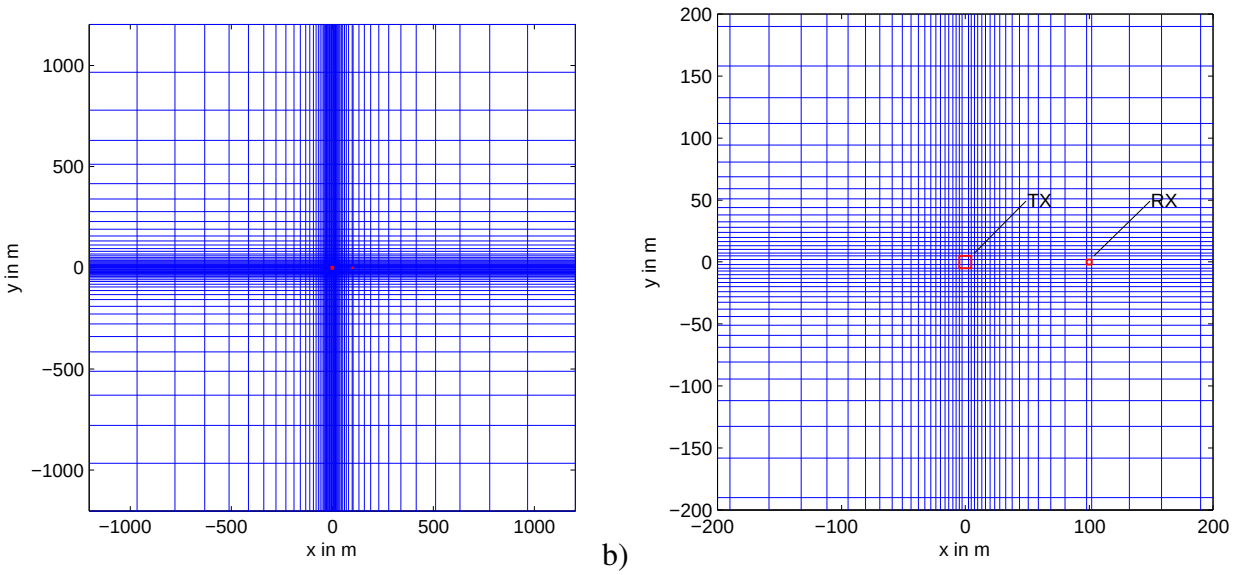

Figure 6: Full extent (a) and section (b) of the finite difference grid ($x - y$-plane, $z = 0$) used for the numerical 3D SLDM experiments.

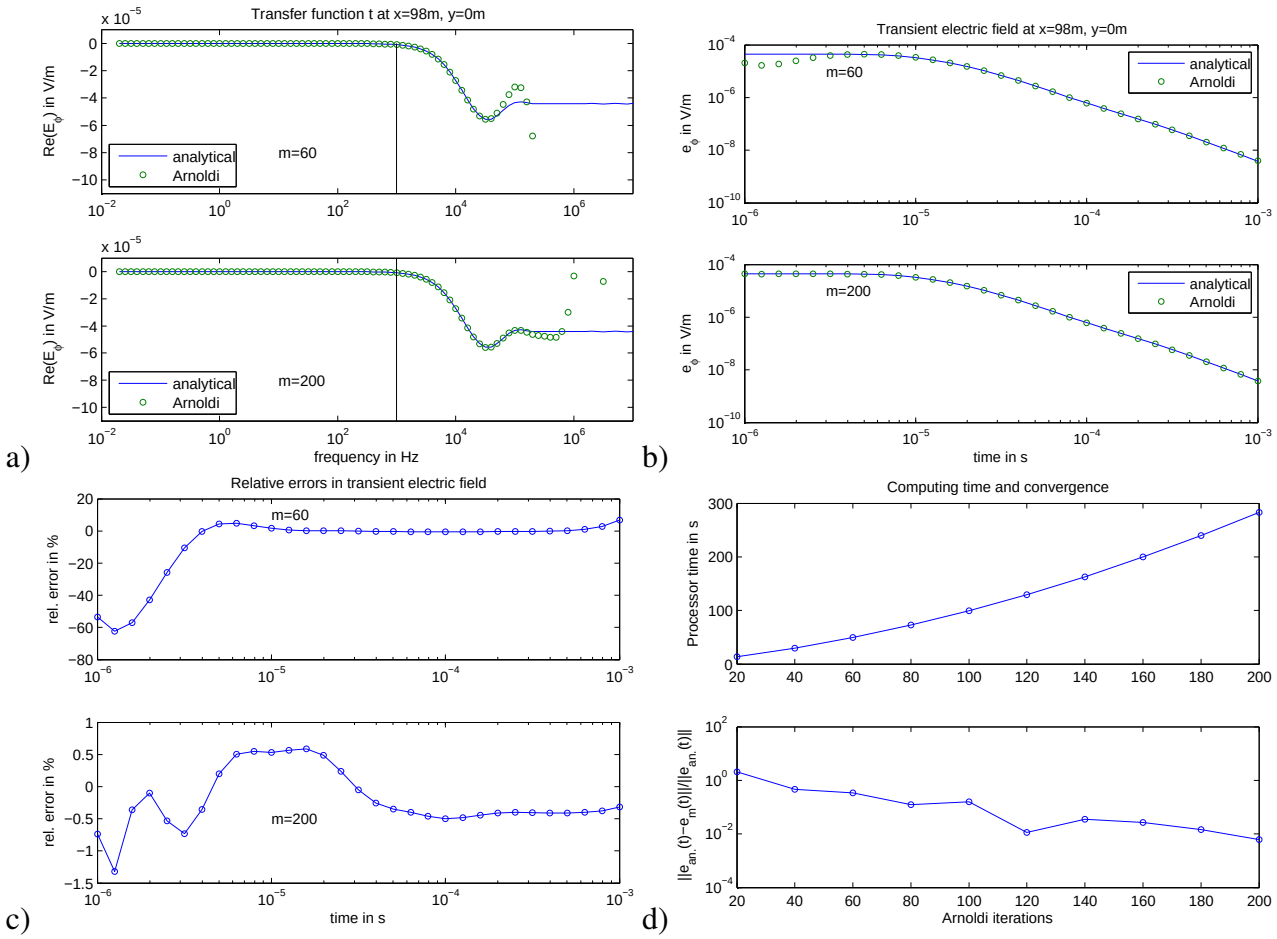

Figure 7: Real part of the transfer function at $x = 98$ m (a), transient electric field $e_m(t)$ (b) for $m = 60$ and $m = 200$ Arnoldi iteration steps, relative error of transient electric field (c), as well as computer time and convergence (d). Reference frequency is 1000 Hz.

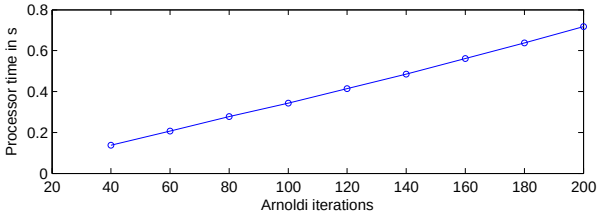

Figure 8: Total processor time for the Fourier synthesis of 110 approximated 3D frequency domain solutions against the number of Arnoldi iterations.

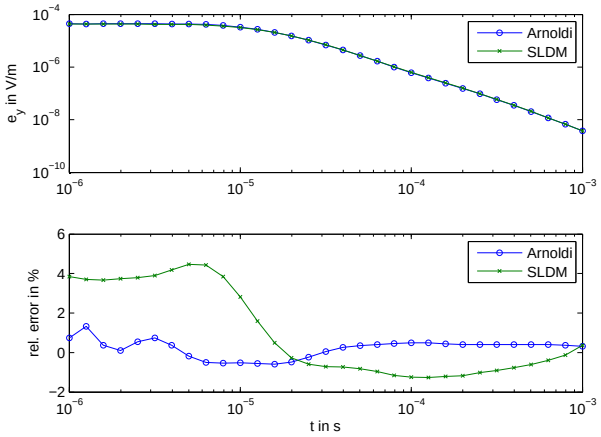

Figure 9: Comparison of transient electric fields (top) and associated relative errors (bottom) for SLDM and Arnoldi solutions at $x = 98$ m.

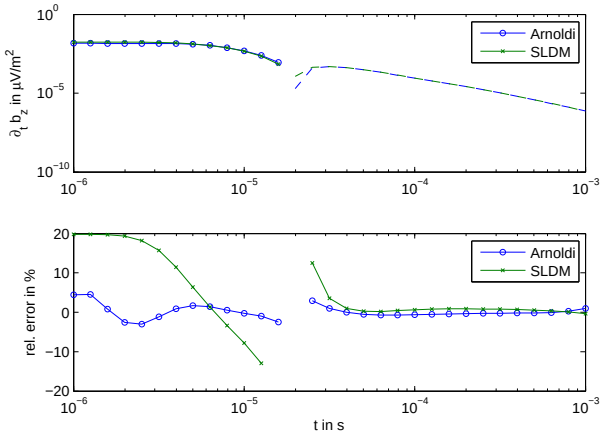

Figure 10: Comparison of transient voltage ($\partial_t b_z$, top) and associated relative errors (bottom) for SLDM and Arnoldi solutions at $x = 100$ m. Note that due to the sign reversal of the voltage signal at $t \approx 2 \cdot 10^{-5}$ s, the relative error yields meaningless results and has therefore been omitted from the figure.

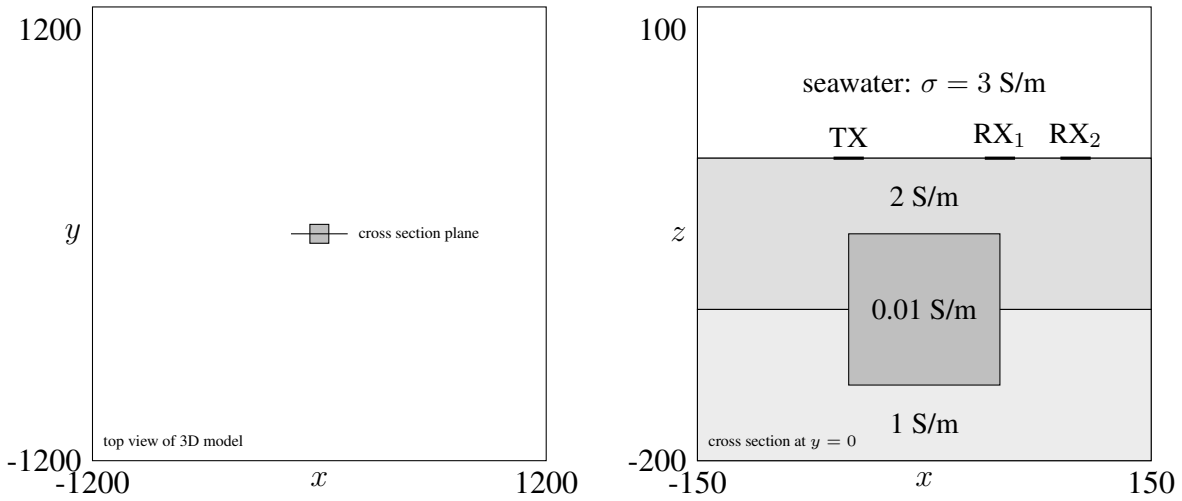

Figure 11: Top view and section of the conductivity structure of the 3D marine model. The seawater layer extends up to 1200 m, the seabottom extends down to -1200 m. We consider transmitter-receiver spacings of 100 and 150 m, respectively.

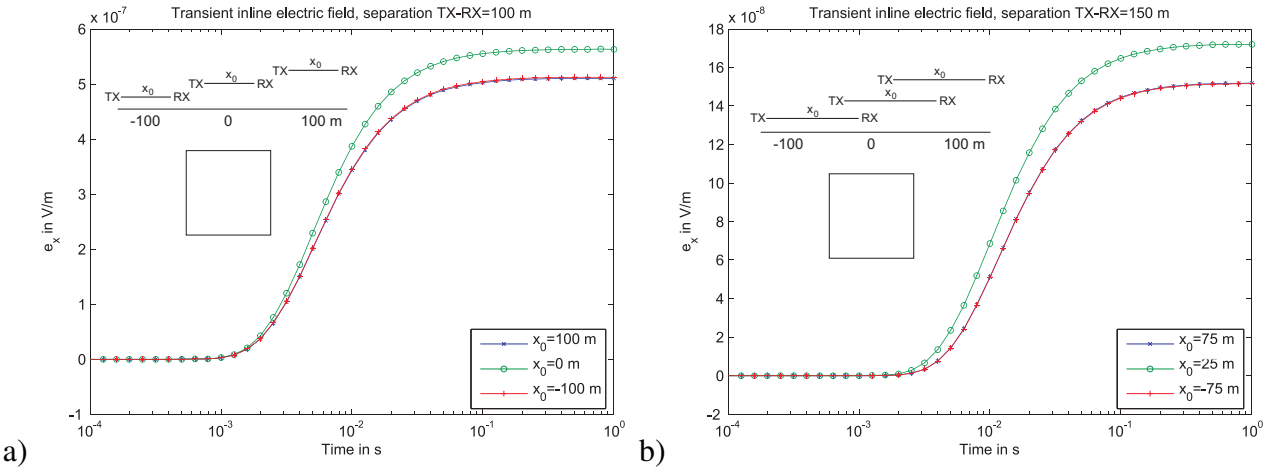

Figure 12: Inline transient electric fields $e_x(t)$ for a current turn-on. Transmitter-receiver spacing is assumed to be 100 m (a) and 150 m (b). Indicated are the transients for various positions of the transmitter-receiver-system midpoint x_0 relative to the position of the resistive body.